A relativistic mean field study of multi-strange system

M. Ikram[1],* S. K. Singh[2],† A. A. Usmani[1],‡ and S. K. Patra[2§]
[1] *Department of Physics, Aligarh Muslim University, Aligarh - 202002, India. and*
[2] *Institute of Physics, Sachivalaya Marg, Bhubaneswar - 751005, India.*
(Dated: June 19, 2014)

We study the binding energies, radii, single-particle energies, spin-orbit potential and density profile for multi-strange hypernuclei in the range of light mass to superheavy region within the relativistic mean field (RMF) theory. The stability of multi-strange hypernuclei as a function of introduced hyperons (Λ and Σ) is investigated. The neutron, lambda and sigma mean potentials are presented for light to superheavy hypernuclei. The inclusion of hyperons affects the nucleon, lambda and sigma spin-orbit potentials significantly. The bubble structure of nuclei and corresponding hypernuclei is studied. The nucleon and lambda halo structure are also investigated. A large class of bound multi-strange systems formed from the combination of nucleons and hyperons (n, p, Λ, Σ^+ and n, p, Λ, Σ^-) is suggested in the region of superheavy hypernuclei which might be stable against the strong decay. These multi-strange systems might be produced in heavy-ion reactions.

PACS numbers:

arXiv:1406.4612v1 [nucl-th] 18 Jun 2014

I. INTRODUCTION

Hypernuclei provide an opportunity to extend our knowledge from normal nucleon-nucleon (NN) interaction to hyperon-nucleon (YN) and hyperon-hyperon (YY) interactions. Many of the single- and few double-lambda hypernuclei have been observed experimentally [1–4], which confirm the existence of S = -1 and -2 systems. Available experimental data is limited for S = -2 sector, and there is no further information for S $\geq$ -3 system. Due to complexity of YY scattering, the production of hypernuclei with strangeness beyond S > -2 is very difficult and not only this, ambiguities also exist in theoretical understanding. It is well known that the hyperon resides at the centre of the nucleus for most of the time, and only two hyperons with opposite spin can stay in s-state. Then further injected hyperons would be sat on p-state would have less binding in comparison to s-state and because of this the production of S $\geq$ -3 systems is difficult. It is obvious, with increasing the strength of strangeness, the hypernuclear physics becomes more complicated. Due to complication and importance of strangeness degree of freedom in bound as well as in infinite nuclear system, this subject has been draw an attention from last few decades [4–44].

The system containing a variety of multi-strange baryons has a unique feature to extend the knowledge on hypernuclear chart with strangeness of S $\geq$ -3 dimension. Many of the theoretical calculations on multi-strange hadronic system have been made which explain the changes and effects occur on bound nuclear system due to injection of Λ hyperon [34–39, 45]. In early investigations within mean field, Rufa *et al.* suggested the stability of multi-lambda hypernuclei and also discussed the pure lambda matter and lambda droplets [45]. The calculations were performed by considering NN and ΛN interactions as a whole for describing the multi-strange system. Even though, they studied the multi-lambda hypernuclei but without including the YY interaction. And the work was limited for medium-heavy spherical nuclei. In present work, we make a complete study of multi-strange hypernuclei within RMF formalism incorporating YY interaction over the periodic chart from light mass to superheavy nuclei by introducing Λ as well as Σ hyperons.

Informations gathered from multi-strange systems are quite useful for studying or simulating the structure of highly dense astrophysical objects. In such a system, there is a possibility of existence of bunch of lambdas which is heavier than nucleons. Not only this, the existence of all variety of hyperons alongwith nucleons is also possible inside the core of neutron star at extreme conditions. In addition to lambda, the production of sigma hypernuclei is more difficult because of $\Sigma-$hyperon has repulsive nature in nuclear matter with potential depth of 30 MeV. But the production of $^{4}_{\Sigma}$He [46, 47], reflects that the many of others $\Sigma-$hypernuclei might be produced. The Λ and Σ^- are appeared at high density around ten times of normal nuclear matter densities at saturation [55]. On the other way, as well as to search the $\Lambda-$ and $\Sigma-$hypernuclei separately, it would be more interesting to look for the bound state of Λ and Σ with nucleons, where $\Lambda N - \Sigma N$ coupling will play an important role for binding mechanism. In this context, the array of stable objects composed of n, p, Λ, Ξ^0, Ξ^- baryons with very high strangeness content and small net charge has been investigated in many Refs. [40–42] within the relativistic mean field model. Not only this, pure hyperonic bound system involving Λ, Ξ^0, Ξ^- hyperons with A $\geq$ 6 has also been suggested [41]. In current study, we search the bound class of multi-strange system by considering Λ, Σ^+ and Σ^- as basic participants in ad-

*Electronic address: ikram@iopb.res.in
†Electronic address: shailesh@iopb.res.in
‡Electronic address: anisul@iucaa.ernet.in
§Electronic address: patra@iopb.res.in

dition to nucleons. The possibilities of bound states of hyperons and nucleons (n, p, Λ, Σ^+ and n, p, Λ, Σ^-) are discussed in this paper in the mass range of superheavy region. It is to expect that the attractive nature of hyperon-hyperon interaction allows to form the bound class of multi-strange system as well as pure hyperonic matter [40–42, 48]. Various calculations have been performed to study the hyperonic system within the RMF with effective interactions [49–53]. The strong strength of attractive YY interaction leads to the formation of a system having nucleons and hyperons or pure hyperonic matter inclusion of all hyperons such as Λ, Σ^0, Σ^+, Σ^-, Ξ^- and Ξ^0 at lower densities [55]. It has to be mention that, the presence of hyperons makes the EOS as softer, and the inclusion of strong YY interaction leads to a further softening of EOS [55]. Incorporation of YY interaction has an impact to study the bound system including hyperons as well as infinite nuclear matter system.

In present work, our motive is to analyze the bulk properties like, binding energies, radii, single-particle energies, spin-orbit potential and density profile for multi-Λ as well as multi-Σ hypernuclei by continuous injection of hyperons with replacing neutrons. The stability of multi-strange system as a function of introduced hyperons from light mass to superheavy region is discussed. The neutron, lambda and sigma mean potentials are investigated for light to superheavy hypernuclei. Nucleon, lambda and sigma spin-orbit potentials are also displayed for different cases of injected hyperons. The bubble structure of nuclei and their disappearance by injection of Λ's is studied. On viewing the density profile, the nucleon and lambda halo nature are reported. The bound class of strange and nonstrange baryons (n, p, Λ, Σ^+ and n, p, Λ, Σ^-) in the mass range of superheavy hypernuclei is predicted which might be produced in heavy ion reactions. The paper is organized as follow: the formalism of RMF model including YY interaction is given in section 2. The results are displayed in section 3. Paper is summarized in section 4.

II. FORMALISM

The structural properties of nuclei are described within the framework of effective mean field interactions in relativistic and non-relativistic approach. RMF model takes care the spin-orbit interaction naturally and produces quite remarkable result over the whole periodic table including superheavy region [62–69]. However, the results produced by original Walecka model was enough qualitatively, but there had some modification by Boguta and Bodmer to match the results with experimental data in quantitative way [69, 70]. This implies that, for a better understanding of nuclear structure studies, it is imperative to include all the possible interactions which affect all the physical observables are being to be calculated. To find the results in quantitative way, we include the σ^* and ϕ mesons which simulate the hyperon-hyperon interaction. Both relativistic (RMF) and non-relativistic (SHF) mean field approaches have been played an interesting as well as successful role in order to explore the hypernuclear systems [37, 45, 56, 57]. The extension towards multi-strange system has been well investigated within RMF however, no experimental data is available for such a high strange system of new kinds as discussed in Refs. [37, 40, 41, 45]. The Lagrangian density for multi-strange hypernuclei is discussed in Refs. [40, 58]. Here, we write the Lagrangian density for multi-strange hypernuclei as given below:

$$\mathcal{L} = \mathcal{L}_N + \mathcal{L}_Y + \mathcal{L}_{YY} \, , Y = \Lambda, \Sigma \, , \tag{1}$$

$$\begin{aligned}
\mathcal{L}_N &= \bar{\psi}_i\{i\gamma^\mu\partial_\mu - M\}\psi_i + \frac{1}{2}(\partial^\mu\sigma\partial_\mu\sigma - m_\sigma^2\sigma^2) \\
&- \frac{1}{3}g_2\sigma^3 - \frac{1}{4}g_3\sigma^4 - g_s\bar{\psi}_i\psi_i\sigma - \frac{1}{4}\Omega^{\mu\nu}\Omega_{\mu\nu} \\
&+ \frac{1}{2}m_\omega^2 V^\mu V_\mu - g_\omega\bar{\psi}_i\gamma^\mu\psi_i V_\mu - \frac{1}{4}B^{\mu\nu}B_{\mu\nu} \\
&+ \frac{1}{2}m_\rho^2\vec{R}^\mu\vec{R}_\mu - \frac{1}{4}F^{\mu\nu}F_{\mu\nu} - g_\rho\bar{\psi}_i\gamma^\mu\vec{\tau}\psi_i\vec{R_\mu} \\
&- e\bar{\psi}_i\gamma^\mu\frac{(1-\tau_{3i})}{2}\psi_i A_\mu \, , \\
\mathcal{L}_Y &= \bar{\psi}_Y\{i\gamma^\mu\partial_\mu - m_Y\}\psi_Y - g_{\sigma Y}\bar{\psi}_Y\psi_Y\sigma \\
&- g_{\omega Y}\bar{\psi}_Y\gamma^\mu\psi_Y V_\mu + \mathcal{L}_{\rho Y} + \mathcal{L}_{AY} \, , \\
\mathcal{L}_{YY} &= \frac{1}{2}(\partial^\mu\sigma^*\partial_\mu\sigma^* - m_{\sigma^*}^2\sigma^{*2}) + \frac{1}{2}m_\phi^2\phi^\mu\phi_\mu \\
&- \frac{1}{4}S^{\mu\nu}S_{\mu\nu} - g_{\sigma^* Y}\bar{\psi}_Y\psi_Y\sigma^* \\
&- g_{\phi Y}\bar{\psi}_Y\gamma^\mu\psi_Y\phi_\mu \, ,
\end{aligned} \tag{2}$$

$$\mathcal{L}_{\rho\Lambda} + \mathcal{L}_{A\Lambda} = 0 \, , \tag{3}$$

because of Λ is neutral and isoscalar

$$\mathcal{L}_{\rho\Sigma} + \mathcal{L}_{A\Sigma} = \bar{\psi}_\Sigma\{g_{\rho\Sigma}\gamma^\mu\vec{\tau}_\Sigma.\vec{R}_\mu + e\frac{(1-\tau_{3\Sigma})}{2}\gamma^\mu A_\mu\}\psi_\Sigma \, , \tag{4}$$

here ψ and ψ_Y denote the Dirac spinors for nucleon and hyperon, whose masses are M and m_Y, respectively. The quantities m_σ, m_ω, m_ρ are the masses for $\sigma-$, $\omega-$ $\rho-$ mesons. The field for the $\sigma-$meson is denoted by σ, $\omega-$meson by V_μ, $\rho-$meson by R_μ. The quantities g_s, g_ω, g_ρ, and $e^2/4\pi$=1/137 are the coupling constants for $\sigma-$, $\omega-$, $\rho-$ and photon fields, respectively. We have g_2 and g_3 self-interaction coupling constants for $\sigma-$mesons. The hyperon-meson coupling constant for strange and non-strange mesons are expressed by $g_{\sigma Y}$, $g_{\omega Y}$, $g_{\sigma^* Y}$ and $g_{\phi Y}$. The field tensors of the vector, isovector mesons and of the electromagnetic field are given by

$$\begin{aligned}
\Omega^{\mu\nu} &= \partial^\mu V^\nu - \partial^\nu V^\mu \, , \\
B^{\mu\nu} &= \partial^\mu R^\nu - \partial^\nu R^\mu \, , \\
F^{\mu\nu} &= \partial^\mu A^\nu - \partial^\nu A^\mu \, , \\
S^{\mu\nu} &= \partial^\mu\phi^\nu - \partial^\nu\phi^\mu \, .
\end{aligned} \tag{5}$$

The classical variational principle is used to solve the Lagrangian and field equations for hypernuclei are obtained. The Dirac equation with potential terms for the nucleon is

$$[-i\alpha.\nabla + \beta(M + S(r)) + V(r)]\psi_i = \epsilon_i\psi_i \ , \qquad (6)$$

where S(r) is the scalar potential of nucleon written as

$$S(r) = g_\sigma\sigma(r) \ , \qquad (7)$$

and V(r) represents the vector potential of nucleon given as

$$V(r) = g_\omega V_0(r) + g_\rho\tau_3 R_0(r) + e\frac{(1-\tau_3)}{2}A_0(r) \ , \qquad (8)$$

where subscript i = n, p in wavefunction denotes the neutron and proton, respectively. The Dirac equation for $\Lambda-$hyperon is

$$[-i\alpha.\nabla + \beta\big(m_\Lambda + S^\Lambda(r)\big) + V^\Lambda(r)]\psi_\Lambda = \epsilon_\Lambda\psi_\Lambda \ , \qquad (9)$$

where $S^\Lambda(r)$ is the scalar potential of $\Lambda-$hyperon given as

$$S^\Lambda(r) = g_{\sigma\Lambda}\sigma(r) + g_{\sigma^*\Lambda}\sigma^*(r) \ , \qquad (10)$$

and $V^\Lambda(r)$ represents the vector potential of $\Lambda-$hyperon written as

$$V^\Lambda(r) = g_{\omega\Lambda}V_0(r) + g_{\phi\Lambda}\phi(r) \ . \qquad (11)$$

The Dirac equation for $\Sigma-$hyperon is

$$[-i\alpha.\nabla + \beta\big(m_\Sigma + S^\Sigma(r)\big) + V^\Sigma(r)]\psi_\Sigma = \epsilon_\Sigma\psi_\Sigma \ , \qquad (12)$$

where $S^\Sigma(r)$ is the scalar potential of $\Sigma-$hyperon given as

$$S^\Sigma(r) = g_{\sigma\Sigma}\sigma(r) + g_{\sigma^*\Sigma}\sigma^*(r) \ , \qquad (13)$$

and $V^\Sigma(r)$ represents the vector potential of $\Sigma-$hyperon written as

$$V^\Sigma(r) = g_{\omega\Sigma}V_0(r) + g_{\rho\Sigma}\tau_{3\Sigma}R_0(r) + e\frac{(1-\tau_{3\Sigma})}{2}A_0(r) + g_{\phi\Sigma}\phi(r) \qquad (14)$$

The Klein-Gordon equations for mesons and Coulomb fields are

$$\begin{aligned}
\{-\triangle + m_\sigma^2\}\sigma(r) &= -g_\sigma\rho_s(r) - g_2\sigma^2(r) - g_3\sigma^3(r) \\
&- g_{\sigma Y}\rho_s^Y(r) \ , \\
\{-\triangle + m_{\sigma^*}^2\}\sigma^*(r) &= g_{\sigma^* Y}\rho_s^Y(r) \ , \\
\{-\triangle + m_\omega^2\}V_0(r) &= g_\omega\rho_v(r) + g_{\omega Y}\rho_v^Y(r) \ , \\
\{-\triangle + m_\phi^2\}\phi_0(r) &= g_{\phi Y}\rho_v^Y(r) \ , \\
\{-\triangle + m_\rho^2\}R_3^0(r) &= g_\rho\rho_3(r) + g_\rho Y\rho_3^Y(r) \ , Y = \Sigma only \ , \\
-\triangle A_0(r) &= e\rho_c(r) + e\rho_c^Y(r) \ , Y = \Sigma only. \qquad (15)
\end{aligned}$$

Here ρ_s, ρ_s^Y and ρ_v, ρ_v^Y are the scalar and vector density for $\sigma-$ and $\omega-$field in nuclear and hypernuclear system which are expressed as

$$\begin{aligned}
\rho_s(r) &= \sum_{i=n,p}\bar{\psi}_i(r)\psi_i(r) \ , \\
\rho_s^Y(r) &= \sum_{Y=\Lambda,\Sigma}\bar{\psi}_Y(r)\psi_Y(r) \ , \\
\rho_v(r) &= \sum_{i=n,p}\psi_i^\dagger(r)\psi_i(r) \ , \\
\rho_v^Y(r) &= \sum_{Y=\Lambda,\Sigma}\psi_Y^\dagger(r)\psi_Y(r) \ . \qquad (16)
\end{aligned}$$

The vector density $\rho_3(r)$ for ρ-field and charge density $\rho_c(r)$ for photon field are expressed by

$$\begin{aligned}
\rho_3(r) &= \sum_{i=n,p}\psi_i^\dagger(r)\gamma^0\tau_{3i}\psi_i(r) \ , \\
\rho_3^Y(r) &= \sum_{Y=\Sigma}\psi_Y^\dagger(r)\gamma^0\tau_{3Y}\psi_Y(r) \ , Y = \Sigma only, \\
\rho_c(r) &= \sum_{i=n,p}\psi_i^\dagger(r)\gamma^0\frac{(1-\tau_{3i})}{2}\psi_i(r) \ , \\
\rho_c^Y(r) &= \sum_{Y=\Sigma}\psi_Y^\dagger(r)\gamma^0\frac{(1-\tau_{3Y})}{2}\psi_Y(r) \ , Y = \Sigma only. \qquad (17)
\end{aligned}$$

The various rms radii are defined as

$$\begin{aligned}
\langle r_p^2\rangle &= \frac{1}{Z}\int r_p^2 d^3r\rho_p \ , \\
\langle r_n^2\rangle &= \frac{1}{N}\int r_n^2 d^3r\rho_n \ , \\
\langle r_m^2\rangle &= \frac{1}{A}\int r_m^2 d^3r\rho \ , \\
\langle r_\Lambda^2\rangle &= \frac{1}{\Lambda}\int r_\Lambda^2 d^3r\rho_\Lambda \ , \\
\langle r_\Sigma^2\rangle &= \frac{1}{\Sigma}\int r_\Sigma^2 d^3r\rho_\Sigma \ , \qquad (18)
\end{aligned}$$

for proton, neutron, matter, lambda and sigma rms radii, respectively and ρ_p, ρ_n, ρ, ρ_Λ and ρ_Σ are their corresponding densities. The charge rms radius can be found from the proton rms radius using the relation $r_{ch} = \sqrt{r_p^2 + 0.64}$ by taking into consideration the finite size of the proton. The total energy of the system is given by

$$\begin{aligned}
E_{total} &= E_{part}(N,Y) + E_\sigma + E_\omega + E_\rho \\
&+ E_{\sigma^*} + E_\phi + E_c + E_{pair} + E_{c.m.}, \qquad (19)
\end{aligned}$$

where $E_{part}(N,Y) = E_{part}(N,\Lambda,\Sigma)$ is the sum of the single particle energies of nucleons (N) and hyperons (Y=Λ,Σ). The other contributions E_σ, E_ω, E_ρ, E_{σ^*}, E_ϕ, E_c, E_{pair} and E_{cm} are from meson fields, Coulomb

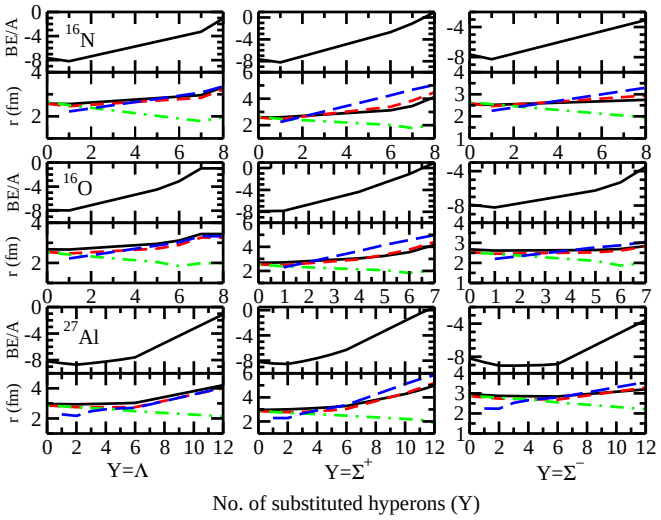

FIG. 1: Energy per particle is shown as a function of substituted hyperons (Λ, Σ^+, Σ^-) for ${}^{16}_{nY}$N, ${}^{16}_{nY}$O and ${}^{27}_{nY}$Al, where Y indicates the injected hyperons (Λ, Σ^+, Σ^-). Total (r_t), charge (r_{ch}), neutron (r_n) and hyperon (r_Y) radii are also displayed as a function of substituted hyperons. Total, charge, neutron and hyperon radii are represented by solid, dashed, dot-dashed and long dashed lines with black, red, green and blue colors, respectively.

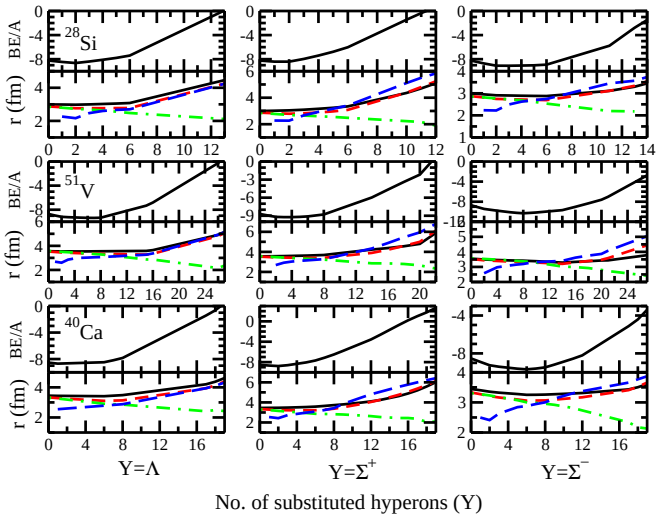

FIG. 2: same as Fig. 1 but for ${}^{28}_{nY}$Si, ${}^{51}_{nY}$V and ${}^{40}_{nY}$Ca.

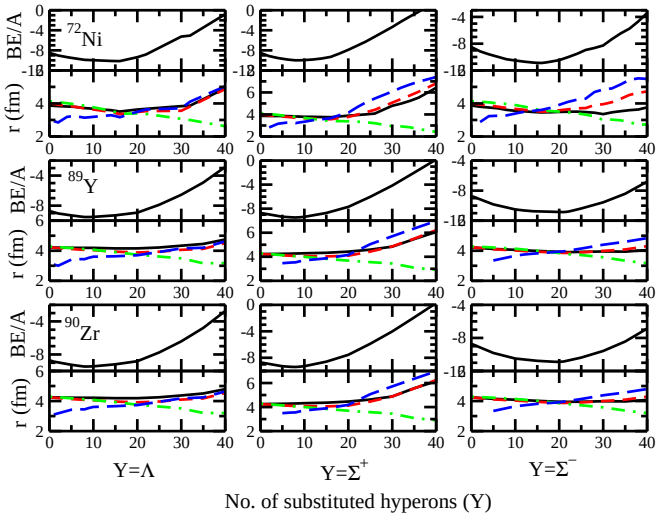

FIG. 3: same as Fig. 1 but for ${}^{72}_{nY}$Ni, ${}^{89}_{nY}$Y and ${}^{90}_{nY}$Zr.

field, pairing energy and the center-of-mass energy, respectively. For present study, we use NL3* nucleon parameter set through out the calculations [71], which produces a good description of nuclear matter as well as finite nuclei including superheavy region [64, 65, 68].

We adopt the relative σ and ω coupling to find the numerical values of hyperon-meson coupling constants. The ratio of meson-hyperon coupling to nucleon-meson coupling is defined by $R_\sigma = g_{\sigma Y}/g_s$, $R_\omega = g_{\omega Y}/g_\omega$, $R_{\sigma^*} = g_{\sigma^* Y}/g_s$ and $R_\phi = g_{\phi Y}/g_\omega$. The relative coupling R_σ, R_ω for Λ and Σ are adopted from Ref. [72]. For meson-hyperon couplings, the naive quark model values are used for vector coupling constants. To incorporate the hyperon-hyperon interaction into the calculation, the relative coupling R_{σ^*}, R_ϕ are taken from Refs. [40, 58, 73]. Here, we consider the coupling strength of sigma-sigma interaction same as lambda-lambda interaction as like as used by Yang, Shen [74] and Miyazaki [75]. That is, $g_{\phi\Lambda} = g_{\phi\Sigma} = \frac{-\sqrt{2}}{3} g_\omega$ from naive quark model and $g_{\sigma^*\Lambda} = g_{\sigma^*\Sigma} = 0.69$ from Ref. [40]. In present calculations, to take care of pairing interaction the constant gap BCS approximation is used and the centre of mass correction is included by the formula $E_{cm} = -(3/4)41A^{-1/3}$.

III. RESULTS AND DISCUSSIONS

A. Binding energies and radii

The stability of multi-strange hypernuclei has been studied by introducing the lambda as well as sigma hyperon by replacing the neutrons. Total and single particle energies for single- Λ and Σ hypernuclei are listed in the Tables I, II, III. Total (r_t), charge (r_{ch}), neutron (r_n) and hyperon (r_Y) radii are also framed in these tables. The single particle energies for s- and p- states are compared with existing data for single−Λ hypernuclei. To check the stability of bound system with high strangeness in respect of injected hyperons, the binding energy per par-

TABLE I: Total and single-particle (for s- and p-state) binding energies and radii are listed for single-Λ hypernuclei. The single-particle energies are compared with available experimental data. Experimental values are given in parenthesis [4, 76].

Hypernuclei	BE	B^s_Λ	B^p_Λ	r_{ch}	r_t	r_p	r_n	r_Λ
${}^{16}_{\Lambda}$N	-130.3091	-14.052(13.76±0.16)	-3.6920(2.84±0.16)	2.562	2.466	2.441	2.509	2.288
${}^{16}_{\Lambda}$O	-126.7055	-14.055(12.5±0.35)	-3.6914(2.5±0.5)	2.664	2.474	2.543	2.419	2.288
${}^{27}_{\Lambda}$Al	-228.2085	-19.840	-8.8560	2.953	2.812	2.845	2.812	2.324
${}^{28}_{\Lambda}$Si	-236.2911	-20.523(16.6±0.2)	-9.3438(7.0±1.0)	2.990	2.825	2.882	2.799	2.313
${}^{32}_{\Lambda}$S	-274.1188	-22.147(17.5±0.5)	-10.455(8.1±0.6)	3.157	2.981	3.055	2.942	2.275
${}^{40}_{\Lambda}$Ca	-347.2458	-20.348(18.7±1.1)	-11.479(11.0±0.6)	3.435	3.286	3.342	3.258	2.600
${}^{48}_{\Lambda}$Ca	-428.2423	-21.700	-13.380	3.435	3.454	3.349	3.554	2.708
${}^{51}_{\Lambda}$V	-456.3979	-22.435(19.97±0.13)	-14.159(11.28±0.6)	3.546	3.490	3.460	3.539	2.727
${}^{56}_{\Lambda}$Fe	-502.2416	-23.542	-15.265	3.642	3.572	3.557	3.609	2.744
${}^{72}_{\Lambda}$Ni	-631.3122	-23.714	-16.640	3.855	3.969	3.782	4.106	2.965
${}^{89}_{\Lambda}$Y	-790.4420	-24.543(23.1±0.5)	-18.095(16.0±1.0)	4.216	4.204	4.145	4.269	3.122
${}^{90}_{\Lambda}$Zr	-797.6272	-24.563	-18.200	4.243	4.218	4.172	4.275	3.141
${}^{132}_{\Lambda}$Sn	-1121.679	-26.159	-20.958	4.677	4.828	4.618	4.967	3.484
${}^{139}_{\Lambda}$La	-1184.506	-25.772(24.5±1.2)	-20.988(20.1±0.4)	4.835	4.895	4.776	4.991	3.624
${}^{208}_{\Lambda}$Pb	-1660.121	-26.935(26.3±0.8)	-23.005(21.3±0.7)	5.490	5.602	5.439	5.718	4.011
${}^{286}_{\Lambda}$114	-2097.325	-26.902	-24.024	6.209	6.279	6.163	6.363	3.269
${}^{298}_{\Lambda}$114	-2169.691	-27.016	-24.143	6.242	6.380	6.198	6.499	3.256
${}^{293}_{\Lambda}$117	-2132.934	-27.016	-24.143	6.248	6.324	6.203	6.412	3.256
${}^{294}_{\Lambda}$118	-2134.069	-27.028	-24.173	6.256	6.327	6.210	6.412	3.284
${}^{292}_{\Lambda}$120	-2108.095	-26.993	-24.213	6.259	6.303	6.213	6.373	3.351
${}^{304}_{\Lambda}$120	-2190.300	-27.215	-24.316	6.296	6.401	6.252	6.506	3.269

ticle (BE/A) are plotted for light to superheavy hypernuclei as displayed in Figs. 1− 6. In case of light mass region the binding energies are enhanced by introducing one or two hyperons and further it goes to reduce. However, for heavy mass region, the BE/A increases with injection of large number of hyperons and form a more bound system than their normal counter parts, for example, inclusion of one lambda increases the binding of ${}^{16}_{n\Lambda}$O, the binding of ${}^{51}_{n\Lambda}$V increases up to the addition of 8 lambdas and the number of injected lambdas for superheavy hypernuclei, ${}^{304}_{n\Lambda}$120, goes to 51. These numbers of lambda hyperons form a multi-strange bound system having maximum stability. Not only lambda, we also look for the stability of multi-sigma hypernuclei. In case of Σ^+, the maximum stability comes forward in comparison to Λ and Σ^- hypernuclei. Because it has a repulsive sigma potential as well as enhance the repulsive Coulomb potential due to its positive charge and as a result the binding of multi-Σ^+ hypernuclei is less. Due to attractive Coulomb potential between Σ^- and proton, the maximum stability for multi-Σ^- hypernuclei is extended. For example, injection of 51 Λ's provide the maximum stability for ${}^{304}_{n\Lambda}$120 and 38 Σ's for ${}^{304}_{n\Sigma^+}$120 while for this nuclei the number of injected Σ^-'s are 70 which produce the maximum stability. By reducing the number of neutrons of nuclei, the neutron radius gradually decreases. On contrary to this, and obviously the lambda, sigma radius increases with increasing the numbers of substituted hyperons (Λ, Σ^+, Σ^-). In some cases, the hyperon radius drastically increases by addition of hyperons, for example, in ${}^{16}_{nY}$O, ${}^{40}_{nY}$Ca, ${}^{51}_{nY}$V, ${}^{72}_{nY}$Ni and so on. This behaviour of radii can be explained by internal shell structure by means of single particle energy levels. The total radius of the hypernuclei initially decreases and after certain limit it goes to increase. This behaviour of r_t indicates that, by addition of hyperons the size of hypernucleus goes to shrink up to a certain limit and then extend the size.

B. Density profile and single particle energies

The nucleon distribution can be explained by density profile which has gross information about the structure of the nucleus. Many of the bulk properties like binding

TABLE II: Total and single-particle (for s- and p-state) binding energies and radii are listed for single-Σ hypernuclei.

Hypernuclei	BE	$B^s_{\Sigma^+}$	$B^p_{\Sigma^+}$	r_{ch}	r_t	r_p	r_n	r_{Σ^+}
$^{16}_{\Sigma^+}$N	-130.7513	-13.631	-4.0893	2.597	2.465	2.478	2.473	2.300
$^{16}_{\Sigma^+}$O	-124.8292	-11.449	-2.4888	2.706	2.488	2.586	2.391	2.363
$^{27}_{\Sigma^+}$Al	-227.6015	-18.490	-8.4594	2.978	2.814	2.872	2.789	2.337
$^{28}_{\Sigma^+}$Si	-234.9222	-18.395	-8.2107	3.017	2.831	2.910	2.779	2.327
$^{32}_{\Sigma^+}$S	-272.8755	-20.031	-9.6561	3.187	2.988	3.086	2.921	2.318
$^{40}_{\Sigma^+}$Ca	-346.4849	-19.008	-10.769	3.457	3.288	3.365	3.239	2.594
$^{48}_{\Sigma^+}$Ca	-430.6025	-23.637	-16.267	3.449	3.451	3.364	3.536	2.757
$^{51}_{\Sigma^+}$V	-457.6058	-23.251	-15.742	3.561	3.488	3.475	3.523	2.746
$^{56}_{\Sigma^+}$Fe	-503.1424	-24.068	-16.321	3.656	3.570	3.572	3.594	2.724
$^{72}_{\Sigma^+}$Ni	-636.0653	-28.154	-21.217	3.866	3.962	3.793	4.089	2.883
$^{89}_{\Sigma^+}$Y	-792.5601	-26.508	-20.686	4.226	4.202	4.155	4.258	3.148
$^{90}_{\Sigma^+}$Zr	-799.4227	-26.162	-20.519	4.253	4.217	4.182	4.263	3.192
$^{132}_{\Sigma^+}$Sn	-1128.721	-31.481	-26.615	4.683	4.823	4.624	4.955	3.455
$^{139}_{\Sigma^+}$La	-1191.296	-29.877	-25.234	4.841	4.891	4.781	4.981	3.536
$^{208}_{\Sigma^+}$Pb	-1665.060	-32.310	-28.540	5.494	5.598	5.443	5.709	3.932
$^{286}_{\Sigma^+}$114	-2075.488	-32.596	-29.719	6.211	6.275	6.165	6.356	4.471
$^{298}_{\Sigma^+}$114	-2148.451	-34.004	-30.666	6.245	6.375	6.200	6.491	4.195
$^{293}_{\Sigma^+}$117	-2110.368	-32.711	-29.779	6.250	6.320	6.205	6.405	4.441
$^{294}_{\Sigma^+}$118	-2112.770	-32.602	-29.695	6.259	6.324	6.214	6.407	4.459
$^{292}_{\Sigma^+}$120	-2087.232	-31.939	-29.210	6.262	6.301	6.217	6.369	4.577
$^{304}_{\Sigma^+}$120	-2168.554	-33.324	-30.155	6.299	6.397	6.254	6.498	4.301

energies, radii, single particle energies and density profile are affected by continuous injection of hyperons. In this regard, we plot the lambda and nucleon density distribution for some light and superheavy hypernuclei as shown in Fig. 8. The nucleon and lambda density distributions are changed by addition of lambdas to normal nuclei. The magnitude of lambda density increases due to increasing number of lambdas. By viewing the density profile, one can examine the most interesting feature of nuclei i.e. bubble structure, which is the measure of depletion of central density. Anomalous behavior of density distribution is observed for bubble nucleus. It shows a dip at the center and a hump nearby to it following a slow decreasing in density to zero at the surface. Some of the interesting examples of bubble nuclei in superheavy region are ^{286}114, ^{292}120, ^{304}120 as reported in Ref. [77].

The existence of bubble structure other than the spherical was first suggested by Wheeler [78] and extensively studied by Wilson [79] however, later by Siemens and Bethe [80]. The explanation on occurrence of bubble nuclei have been made using several models like, independent particle and Hartree-Fock Model [81, 82]. One of the interesting thing in this context is, it is not confined to a particular region but have the possibility for light mass to superheavy region. One may expect that, the mechanism behind the formation of bubble structure is the depopulation of s levels and as a result due to less bound lower s levels the radius increases and subsequently, central part of density decreases [83, 84]. The bubble and semi-bubble structure for superheavy and hyperheavy mass region have been reported in Refs. [83, 85]. Not only depopulation of s-levels is responsible to make the hollow of central region but this may also be interpreted by s-d orbital inversion as discussed by Zhao *et al.* and E Khan *et al.* [86, 87]. In quantitative way, the amount of bubble effect can be measured by calculating depletion fraction (DF) using the relation [86, 87];

$$(DF)_\alpha = \frac{(\rho_{max})_\alpha - (\rho_{cen})_\alpha}{(\rho_{max})_\alpha} \times 100,$$

where ρ_{max}, ρ_{cen} represent the maximum and central density, respectively and α denotes the neutron and proton. Not only syperheavy but some medium-heavy nuclei also have a good amount of depletion fraction as tabulated in Table IV. The depletion of central density is decreased or completely reduced by injection of hyperons to

TABLE III: Total and single-particle (for s- and p-state) binding energies and radii are listed for single-Σ hypernuclei.

Hypernuclei	BE	$B^s_{\Sigma^-}$	$B^p_{\Sigma^-}$	r_{ch}	r_t	r_p	r_n	r_{Σ^-}
${}^{16}_{\Sigma^-}$N	-131.8578	-14.551	-5.1063	2.524	2.469	2.401	2.545	2.321
${}^{16}_{\Sigma^-}$O	-131.0975	-17.268	-7.2379	2.618	2.460	2.493	2.450	2.259
${}^{27}_{\Sigma^-}$Al	-233.6156	-24.192	-13.646	2.918	2.803	2.810	2.831	2.293
${}^{28}_{\Sigma^-}$Si	-242.9184	-26.117	-15.343	2.954	2.813	2.845	2.815	2.279
${}^{32}_{\Sigma^-}$S	-281.4468	-28.488	-16.885	3.118	2.968	3.015	2.963	2.211
${}^{40}_{\Sigma^-}$Ca	-355.4514	-27.717	-19.053	3.405	3.277	3.311	3.274	2.546
${}^{48}_{\Sigma^-}$Ca	-433.1445	-25.891	-17.289	3.412	3.452	3.326	3.570	2.581
${}^{51}_{\Sigma^-}$V	-463.4586	-28.799	-20.399	3.523	3.484	3.437	3.552	2.621
${}^{56}_{\Sigma^-}$Fe	-510.6156	-31.242	-23.060	3.619	3.566	3.534	3.621	2.667
${}^{72}_{\Sigma^-}$Ni	-637.4301	-27.808	-21.023	3.836	3.970	3.762	4.120	2.922
${}^{89}_{\Sigma^-}$Y	-798.7386	-34.723	-27.787	4.196	4.198	4.125	4.277	2.919
${}^{90}_{\Sigma^-}$Zr	-806.6424	-35.459	-28.481	4.223	4.212	4.152	4.282	2.912
${}^{132}_{\Sigma^-}$Sn	-1129.498	-34.684	-29.323	4.661	4.825	4.602	4.973	3.319
${}^{139}_{\Sigma^-}$La	-1195.729	-37.227	-32.361	4.820	4.891	4.760	4.995	3.474
${}^{208}_{\Sigma^-}$Pb	-1679.528	-42.618	-38.066	5.475	5.596	5.423	5.720	3.626
${}^{286}_{\Sigma^-}$114	-2096.123	-47.418	-43.950	6.194	6.271	6.148	6.362	4.130
${}^{298}_{\Sigma^-}$114	-2166.315	-46.453	-43.118	6.228	6.374	6.183	6.499	4.208
${}^{293}_{\Sigma^-}$117	-2120.401	-48.304	-44.889	6.233	6.316	6.188	6.411	4.161
${}^{294}_{\Sigma^-}$118	-2123.234	-48.646	-45.247	6.242	6.320	6.197	6.413	4.168
${}^{292}_{\Sigma^-}$120	-2099.320	-49.699	-46.318	6.246	6.296	6.200	6.373	4.112
${}^{304}_{\Sigma^-}$120	-2189.437	-48.468	-45.219	6.282	6.395	6.237	6.505	4.250

TABLE IV: Total depletion fraction (D.F.) (in %) as a measure of depletion of central density for nucleon distribution is listed for some selected bubble nuclei and their corresponding multi-strange hypernuclei.

Nuclei	D.F.	Hypernuclei	D.F.	Hypernuclei	D.F.	Hypernuclei	D.F.	Hypernuclei	D.F.	Hypernuclei	D.F.
^{16}O	15.11	${}^{16}_{1\Lambda}$O	4.81	${}^{16}_{5\Lambda}$O	0.0	${}^{16}_{6\Lambda}$O	0.0	${}^{16}_{7\Lambda}$O	0.0	${}^{16}_{8\Lambda}$O	0.0
^{22}O	26.22	${}^{22}_{1\Lambda}$O	23.37	${}^{22}_{2\Lambda}$O	17.94	${}^{22}_{4\Lambda}$O	12.63	${}^{22}_{5\Lambda}$O	8.42	${}^{22}_{12\Lambda}$O	0.0
^{28}Si	41.45	${}^{28}_{1\Lambda}$Si	38.59	${}^{28}_{2\Lambda}$Si	33.75	${}^{28}_{4\Lambda}$Si	25.77	${}^{28}_{6\Lambda}$Si	18.35	${}^{28}_{7\Lambda}$Si	0.0
^{34}Si	15.28	${}^{34}_{1\Lambda}$Si	12.57	${}^{34}_{2\Lambda}$Si	9.82	${}^{34}_{6\Lambda}$Si	47.67	${}^{34}_{8\Lambda}$Si	49.98	${}^{34}_{18\Lambda}$Si	0.0
^{46}Ar	36.03	${}^{46}_{1\Lambda}$Ar	0.0	${}^{46}_{2\Lambda}$Ar	0.0	${}^{46}_{4\Lambda}$Ar	0.0	${}^{46}_{6\Lambda}$Ar	0.0	${}^{46}_{26\Lambda}$Ar	0.0
^{90}Zr	19.29	${}^{90}_{5\Lambda}$Zr	18.75	${}^{90}_{10\Lambda}$Zr	21.03	${}^{90}_{15\Lambda}$Zr	27.33	${}^{90}_{20\Lambda}$Zr	1.62	${}^{90}_{25\Lambda}$Zr	2.28
^{138}Ce	44.91	${}^{138}_{10\Lambda}$Ce	16.02	${}^{138}_{20\Lambda}$Ce	38.35	${}^{138}_{30\Lambda}$Ce	31.66	${}^{138}_{40\Lambda}$Ce	10.73	${}^{138}_{70\Lambda}$Ce	0.0
^{200}Hg	42.35	${}^{200}_{10\Lambda}$Hg	34.42	${}^{200}_{30\Lambda}$Hg	23.47	${}^{200}_{50\Lambda}$Hg	54.0	${}^{200}_{70\Lambda}$Hg	15.85	${}^{200}_{90\Lambda}$Hg	5.08
^{206}Hg	34.57	${}^{206}_{10\Lambda}$Hg	37.05	${}^{206}_{30\Lambda}$Hg	28.56	${}^{206}_{50\Lambda}$Hg	52.69	${}^{206}_{70\Lambda}$Hg	51.14	${}^{206}_{90\Lambda}$Hg	0.0
^{286}114	24.62	${}^{286}_{10\Lambda}$114	20.57	${}^{286}_{20\Lambda}$114	16.09	${}^{286}_{30\Lambda}$114	11.99	${}^{286}_{40\Lambda}$114	8.54	${}^{286}_{50\Lambda}$114	4.19
^{298}114	0.0	${}^{298}_{10\Lambda}$114	22.25	${}^{298}_{20\Lambda}$114	22.96	${}^{298}_{30\Lambda}$114	18.36	${}^{298}_{40\Lambda}$114	13.04	${}^{298}_{50\Lambda}$114	10.52
^{293}117	25.17	${}^{293}_{10\Lambda}$117	22.44	${}^{293}_{20\Lambda}$117	18.35	${}^{293}_{30\Lambda}$117	15.83	${}^{293}_{40\Lambda}$117	10.21	${}^{293}_{50\Lambda}$117	9.66
^{294}118	25.49	${}^{294}_{10\Lambda}$118	22.93	${}^{294}_{20\Lambda}$118	18.18	${}^{294}_{30\Lambda}$118	16.02	${}^{294}_{40\Lambda}$118	10.38	${}^{294}_{50\Lambda}$118	10.70
^{292}120	30.85	${}^{292}_{10\Lambda}$120	23.59	${}^{292}_{20\Lambda}$120	19.96	${}^{292}_{30\Lambda}$120	14.74	${}^{292}_{40\Lambda}$120	10.96	${}^{292}_{50\Lambda}$120	9.78
^{304}120	0.89	${}^{304}_{10\Lambda}$120	28.37	${}^{304}_{20\Lambda}$120	21.59	${}^{304}_{30\Lambda}$120	20.40	${}^{304}_{40\Lambda}$120	14.14	${}^{304}_{50\Lambda}$120	7.54

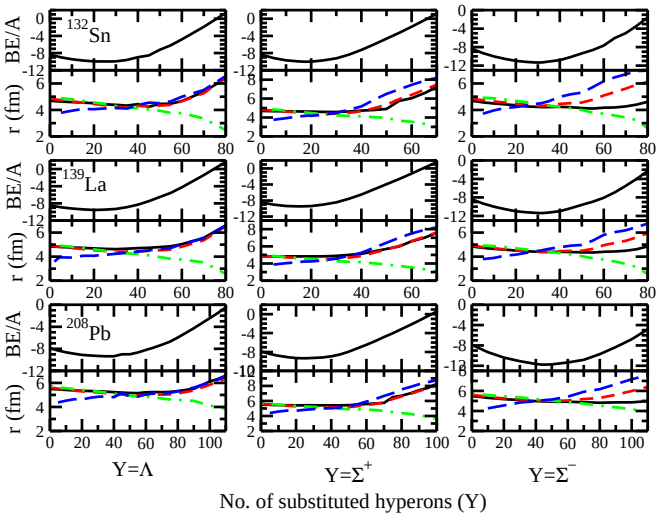

FIG. 4: same as Fig. 1 but for ${}^{132}_{nY}$Sn, ${}^{139}_{nY}$La and ${}^{208}_{nY}$Pb.

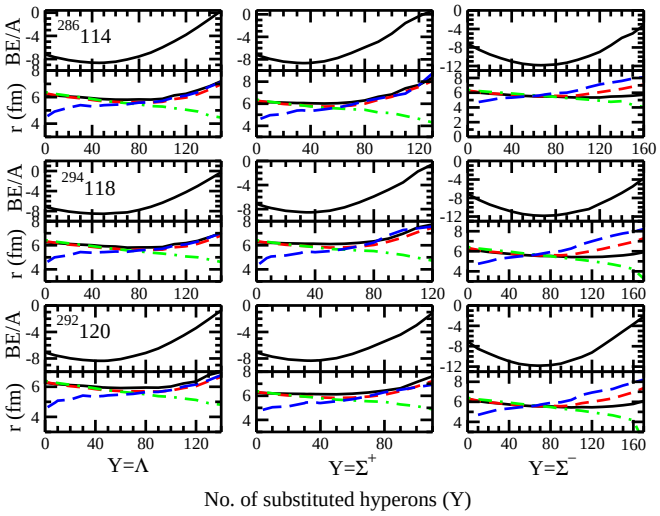

FIG. 5: same as Fig. 1 but for ${}^{286}_{nY}$114, ${}^{294}_{nY}$118 and ${}^{292}_{nY}$120.

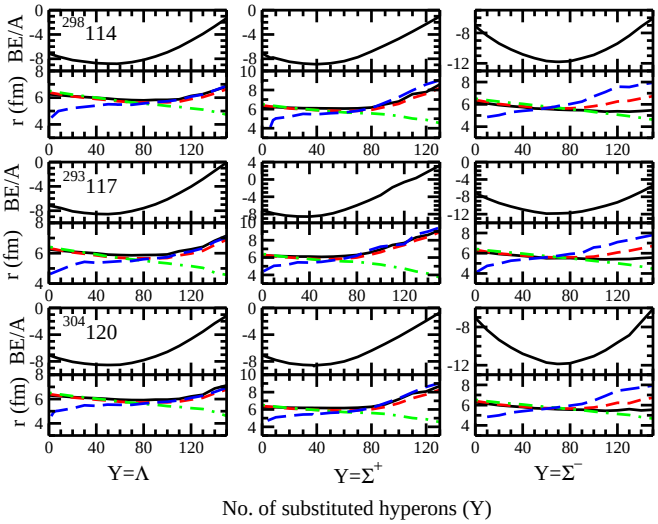

FIG. 6: same as Fig. 1 but for ${}^{298}_{nY}$114, ${}^{293}_{nY}$117 and ${}^{304}_{nY}$120.

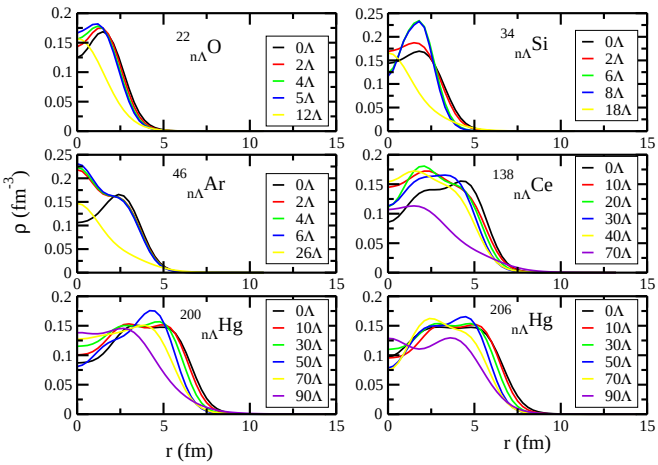

FIG. 7: To see the depletion fraction especially for light bubble nuclei, the nucleon density is displayed for ${}^{22}_{n\Lambda}$O, ${}^{34}_{n\Lambda}$Si, ${}^{46}_{n\Lambda}$Ar, ${}^{138}_{n\Lambda}$Ce, ${}^{200}_{n\Lambda}$Hg and ${}^{206}_{n\Lambda}$Hg.

normal nuclei as shown in Fig. 7, 8. For the case of ^{16}O, the depletion fraction is 15.11, and this amount reaches to 4.81 for ${}^{16}_{\Lambda}$O and ultimately becomes zero for ${}^{16}_{5\Lambda}$O hypernucleus as given in Table IV. In the same way, ^{286}114 has a big amount of DF as 24.62 and this value reduced to 4.19 by injecting 50 lambdas to ^{286}114 with replacing neutrons. In this way, we can say that the addition of lambdas to nuclei has the ability to remove the bubble structure partially or fully which is appeared in normal nuclei. The effect of lambdas on density profile by means of effect on depletion fraction are shown in Figs. 7, 8. Some interesting bubble nuclei like as ^{22}O, ^{34}Si, ^{46}Ar, ^{138}Ce, ^{200}Hg and ^{206}Hg are considered as to reveal the effect of lambdas on density profile. It is evident from Figs. 7, 8 and Table IV that the injection of lambdas affects the DF partially or completely and as a result the amount of DF becomes very small or zero. In the same time, the magnitude of nucleon density decreases because of decreasing number of neutrons. For example, for ^{46}Ar, the DF is 36 and this amount becomes zero by injection of 2 or more lambdas to the core nucleus. This happens because of lambda particle resides at the centre of the nucleus and attracts the surrounding nucleon towards the centre and as a result central density becomes high and the hollow part of the centre is filled by partially or completely. This is one of the most important implication of hyperon to nuclei for removing the bubble nature of nuclei.

The other prospects of density profile is to analyze the

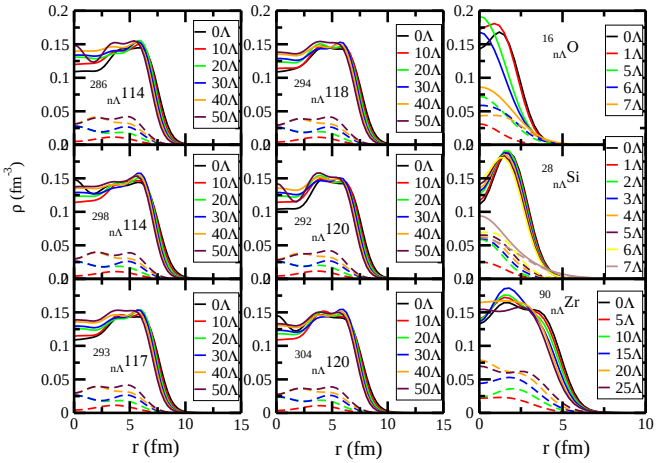

FIG. 8: Nucleon and lambda densities for non-strange to multi-strange nuclei are displayed for ${}^{286}_{n\Lambda}114$, ${}^{298}_{n\Lambda}114$, ${}^{293}_{n\Lambda}117$, ${}^{294}_{n\Lambda}118$, ${}^{292}_{n\Lambda}120$, ${}^{304}_{n\Lambda}120$, ${}^{16}_{n\Lambda}$O, ${}^{28}_{n\Lambda}$Si and ${}^{90}_{n\Lambda}$Zr. Solid lines represent the nucleon density and lambda densities represented by dashed lines.

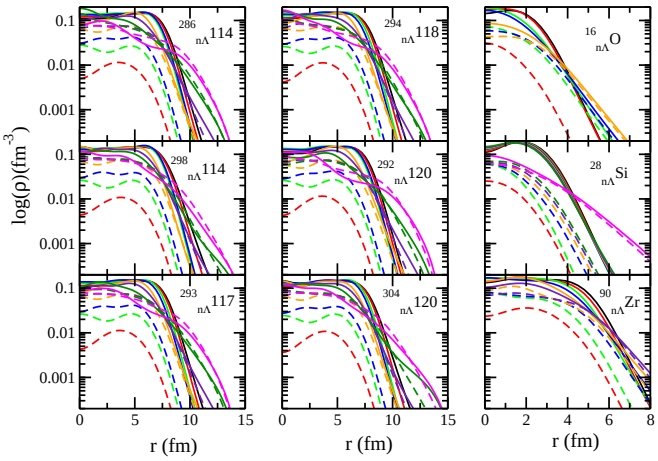

FIG. 9: The nucleon and lambda densities of Figure 8 are plotted in logarithm scale to analyze the nucleon and lambda halo nature for ${}^{286}_{n\Lambda}114$, ${}^{298}_{n\Lambda}114$, ${}^{293}_{n\Lambda}117$, ${}^{294}_{n\Lambda}118$, ${}^{292}_{n\Lambda}120$, ${}^{304}_{n\Lambda}120$, ${}^{16}_{n\Lambda}$O, ${}^{28}_{n\Lambda}$Si and ${}^{90}_{n\Lambda}$Zr. In the same way as Fig 8, the nucleon and lambda densities are represented by solid and dashed lines, respectively.

halo nature of nucleon and lambda. It is one of the interesting character of the nuclei which makes differ from the normal nuclei. The halo nuclei has slowly decaying exponential tails extending beyond the size of the nucleus. To examine the halo nature of nucleon and Λ hyperon, we plot the density in logarithm scale. The halo nature is identified by wide space extension of density distribution. It is evident from Fig. 9 that the ${}^{16}_{7\Lambda}$O, ${}^{28}_{7\Lambda}$Si, ${}^{90}_{40\Lambda}$Zr and ${}^{90}_{50\Lambda}$Zr show nucleon and lambda halo in light medium mass region. In superheavy mass region, the hypernu-

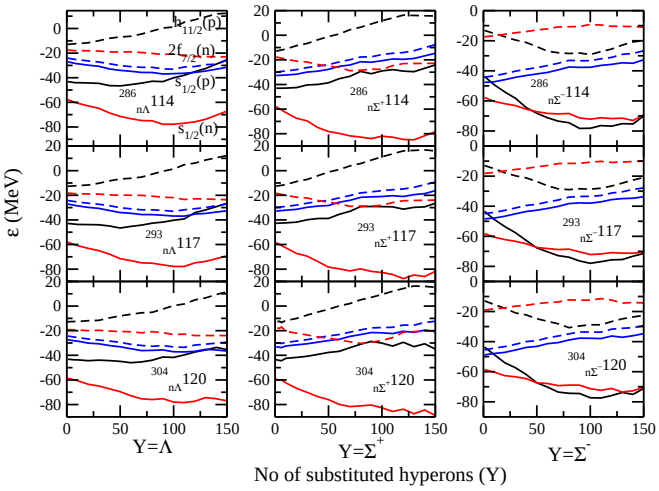

FIG. 10: The first occupied and higher orbits of neutron and proton are shown for ${}^{286}_{n\Lambda}114$, ${}^{293}_{n\Lambda}117$, ${}^{304}_{n\Lambda}120$ and ${}^{286}_{n\Sigma^+}114$, ${}^{293}_{n\Sigma^+}117$, ${}^{304}_{n\Sigma^+}120$ and ${}^{286}_{n\Sigma^-}114$, ${}^{293}_{n\Sigma^-}117$, ${}^{304}_{n\Sigma^-}120$ as a function of substituted hyperons (Λ, Σ^+ and Σ^-) with replacing neutrons. Solid lines with red, black and blue color represent the $1s_{1/2}$ level for neutron, proton and hyperon, respectively. The higher neutron ($2f_{7/2}$), proton ($1h_{11/2}$) and hyperon ($1p_{3/2}$) levels are represented by dashed line with red, black and blue color, respectively.

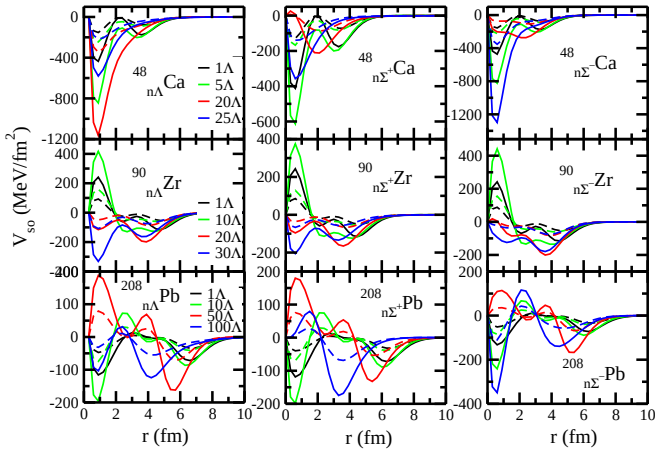

FIG. 11: Radial dependence of spin-orbit potential for nucleon (V_{so}^{N}) and hyperons (V_{so}^{Λ}, $V_{so}^{\Sigma^+}$, $V_{so}^{\Sigma^-}$) are plotted for ${}^{48}_{n\Lambda}$Ca, ${}^{90}_{n\Lambda}$Zr, ${}^{208}_{n\Lambda}$Pb and ${}^{48}_{n\Sigma^+}$Ca, ${}^{90}_{n\Sigma^+}$Zr, ${}^{208}_{n\Sigma^+}$Pb and ${}^{48}_{n\Sigma^-}$Ca, ${}^{90}_{n\Sigma^-}$Zr, ${}^{208}_{n\Sigma^-}$Pb. Nucleon and hyperon spin-orbit potentials are represented by solid and dashed lines, respectively.

clei ${}^{286}_{n\Lambda}114$, ${}^{298}_{n\Lambda}114$, ${}^{293}_{n\Lambda}117$, ${}^{294}_{n\Lambda}118$, ${}^{292}_{n\Lambda}120$, ${}^{304}_{n\Lambda}120$ with 140, 160 lambdas reveal the nucleon and lambda halo as shown in Fig. 9. In general, the addition of excessive lambdas corresponding to nuclei exhibit the neutron and lambda halo nature. The reason is simple, the majority of lambda hyperons push out the nucleon towards periphery and formed nucleon halo. The successive ad-

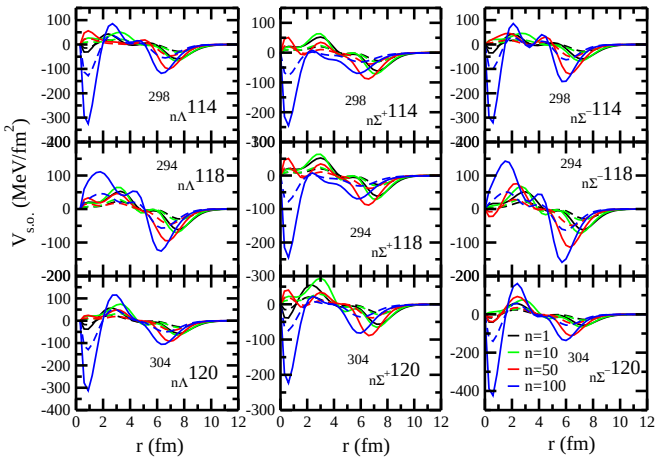

FIG. 12: Same as Fig. 11 but for superheavy mass region ${}^{298}_{n\Lambda}114$, ${}^{294}_{n\Lambda}118$, ${}^{304}_{n\Lambda}120$ and ${}^{298}_{n\Sigma^+}114$, ${}^{294}_{n\Sigma^+}118$, ${}^{304}_{n\Sigma^+}120$ and ${}^{298}_{n\Sigma^-}114$, ${}^{294}_{n\Sigma^-}118$, ${}^{304}_{n\Sigma^-}120$.

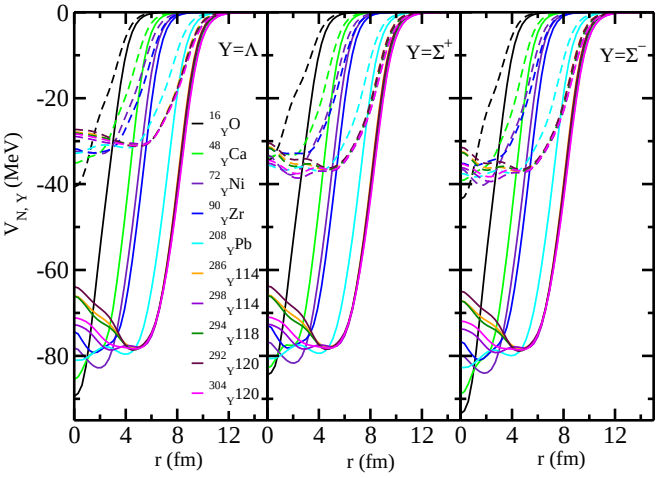

FIG. 13: The neutron (V_N) and hyperon ($V_Y = V_\Lambda, V_\Sigma^+, V_\Sigma^-$) mean potentials are plotted for ${}^{16}_{Y}$O, ${}^{48}_{Y}$Ca, ${}^{72}_{Y}$Ni, ${}^{90}_{Y}$Zr, ${}^{208}_{Y}$Pb, ${}^{286}_{Y}114$, ${}^{298}_{Y}114$, ${}^{294}_{Y}118$, ${}^{292}_{Y}120$, ${}^{304}_{Y}120$. Neutron and hyperon mean potentials are represented by solid and dashed lines, respectively.

dition of hyperons by replacing the neutrons provide the deep binding of neutrons due to the symmetry energy. Because of successive addition of Λ to the nuclei the Λ separation energy reduces and weak binding of hyperon levels leads to the halo nature of hyperon as discussed in Ref. [88]. The Λ density is found to be maximum near the center from where it pushes the nucleons towards the low density regions both at the periphery and at the center. And due to this, the bubble structure is disappeared partially or completely and also Λ and nucleon halo structure is seen.

Any kinds of change in a system is directly reflected

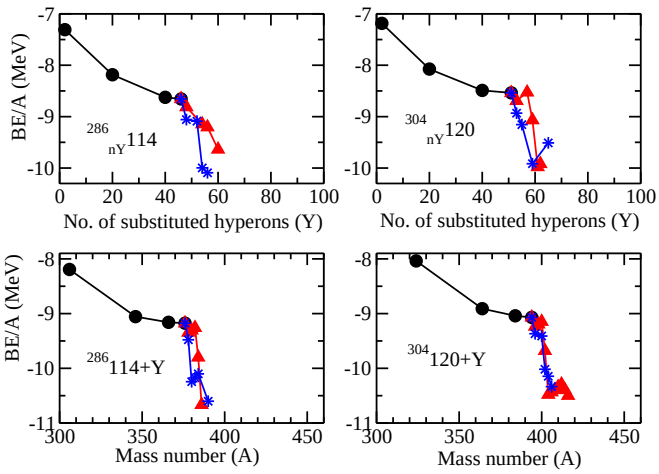

FIG. 14: Binding energy per baryon (BE/A) as a function of substituted hyperons for ${}^{286}_{nY}114$ and ${}^{304}_{nY}120$ is displayed in upper portion of the figure. Binding energy per baryon (BE/A) as a function of mass number A for ${}^{286}114$+Y and ${}^{304}120$+Y, where Y=Λ+Σ^+, Λ+Σ^- is presented in lower part of the figure. The solid circles in black color represent the binding for lambda, while the solid triangles in red color denote the binding for added Σ^+'s and the stars in blue color represent the binding by added Σ^-'s.

from the single particle energy levels. To analyze the impact of hyperon on single particle energy levels, we plot the first and some higher filled neutron, proton and hyperon (Λ, Σ^+, Σ^-) levels as a function of substituted hyperons for superheavy region. In case of lambda hypernuclei, the first filled neutron level goes deeper and first proton level also feels the attraction. By decreasing the number of neutrons (injection of hyperons) the impact of Coulomb repulsion becomes higher and the upper proton level goes to unbound. The deep binding of neutron level is because of decresing in symmetry energy due to substitution of neutron by Λ as discussed in Ref. [89]. For Σ^+ case, the attraction is less and Coulomb repulsion becomes high enough because of positive charge of Σ^+ hyperon. On the other hand, due to Σ^- hyperons the proton as well as neutron levels feel more bound. Here in this case, the proton levels are bound enough than their neutron levels as shown in Fig. 10. The lambda energy levels feel to be constant or mild attractive with the function of injected lambdas. On contrary to this, the sigma levels go towards less binding which is clearly reflected from Fig. 10.

C. Spin-orbit and mean potentials

In order to investigate the structural properties of nuclei, the spin-orbit interaction plays a significant role to produce the results in quantitative way. It is the beauty of RMF in which the spin-orbit splitting develops nat-

urally by the exchange of scalar and vector mesons and this is not limited only for nuclei but exists in hypernuclei also [90–92]. However, the spin-orbit potential in hypernuclei is weaker than their normal nuclear case as demonstrated in Refs. [73, 93, 94]. It is clearly shown in Figs. 11, 12 that the spin-orbit potential for hyperon is weaker than their normal counter parts and these results are consistent with existing predictions [73, 93, 94]. In this work, we study the spin-orbit potential for nucleons (V_{so}^{N}) as well as hyperons (V_{so}^{Λ}, $V_{so}^{\Sigma^+}$, $V_{so}^{\Sigma^-}$) of hypernuclei for different cases of hyperons. The effect of large number of injected hyperons on spin-orbit potentials is significantly investigated and plotted in Figs. 11, 12 for medium to superheavy multi-strange hypernuclei.

The neutron (V_N), lambda (V_Λ) and sigma (V_Σ^+, V_Σ^-) mean potentials are also investigated and plotted in Fig. 13 for light to superheavy hypernuclei. The mean potential depth of lambda and sigma is found to be 30 MeV, which is in agreement of existing calculations [73]. The neutron potential depth for light hypernuclei lies approx 80 MeV, which reduces to around 64 MeV for superheavy hypernuclei. The shape of hyperon potential looks like to be same as neutron potential but only the amount of depth is different. It is to be notice that the neutron potential looks like as V-shape type and shows the maximum depth around 78 MeV at r=4 fm, while this amount of depth is reduced to around 65 MeV at r=0 fm. This is an indication of relatively low concentration of the particles at central region (r=0) which is the direct consequence of formation of bubble structure.

D. Possible bound states of multi-strange systems

The extension towards the systems of large strangeness has firstly been investigated in Refs. [40–42, 45]. Some of the theoretical calculations have been made and suggested the bound class of objects composed of neutrons, protons, Λ's and Ξ's for light-medium nuclei [40, 41]. In this context, we deal the multi-strange system with other heavy hyperon. The systems of high strangeness developed by addition of Λ's have more bound nature than their normal nuclear counter parts. As we have seen in Figs. 1−6, where the BE/A increases for a certain limit of lambda particle and shows the maximum stability for a particular system. Here, we try to suggest the stable systems having more heavier hyperons including lambdas for example, Σ^+ and Σ^-. In this connection, we examine some combinations of n, p, Λ, Σ^+ and n, p, Λ, Σ^- in the range of superheavy nuclei by two ways. In first one, we add the hyperons with replacing neutrons by staying the mass number as constant as shown in upper part of Fig. 14 while in second one, we add the hyperons in ordinary nuclei with increasing mass number and as a result the bound system with high strangeness is suggested. We frame the bound state in such a way that after getting the maximum stability by addition of Λ's, the Σ^+ and Σ^- hyperons are injected which further increase the binding of the system as shown in Fig. 14. The upper portion of Fig. 14 indicates that the more deeply bound than systems of same A are presented with replacing the neutrons by Λ's and Σ's. The following possible combinations are presented as n_Λ=46, with n_{Σ^+}=2, 8, 10, 14 and n_{Σ^-}=2, 6, 8, 10 by maintaining A=286 for ${}^{286}_{nY}114$. For ${}^{304}_{nY}120$ hypernuclei with maintaining the mass number A=304, the possible combinations are n_Λ=51, with n_{Σ^+}=2, 6, 8, 10, 11 and n_{Σ^-}=2, 4, 8, 14. In other way, the possible combinations of nucleons and hyperons by adding the hyperons with increasing the mass number for ${}^{286}114$+Y are given as follow; n_Λ=90, with n_{Σ^+}=2, 4, 6, 8, 10 and n_{Σ^-}=2, 4, 6, 8, 14. In the same way for ${}^{304}120$+Y, the combinations are given as n_Λ=90, with n_{Σ^+}=2, 4, 6, 8, 10, 14, 16, 18, 20, 22 and n_{Σ^-}=2, 6, 8, 10, 12 which have increasing binding for a particular system.

IV. SUMMARY AND CONCLUSIONS

It is really true that, the RMF produces quite excellent result not only for normal nuclei but hypernuclei also. We demonstrate the various physical properties of hypernuclei within the RMF and also see the effects of successive addition of hyperons to nuclear bound system. In which, we expose how does the binding energies, radii, density and single particle energies are affected by continuous injection of hyperons ($\Lambda, \Sigma^+, \Sigma^-$).

In this paper, we study the bulk properties as well as check the stability of hypernuclei within the RMF for a wide spectrum from light mass to superheavy region. We investigate the binding energies, radii and single particle energies as a function of successive added Λ's, Σ^+'s and Σ^-'s. The stability of multi-strange hypernuclei is investigated as a function of added hyperons from light mass to superheavy region. A variation in achieving the maximum stability for a particular system is observed for injection of different kinds of hyperons. The study of bubble structure of the nuclei and the disappearance of bubble nature by addition of hyperons to normal nuclei is presented. The amount of depletion fraction of the nuclei is reduced by successive addition of hyperons. Removing the bubble structure of nuclei by injection of lambdas is an important implication of strange baryons to ordinary nuclei. The nucleon and hyperon halo structure is also investigated. The study of single-particle energy levels of Λ, Σ^+ and Σ^-hypernuclei is presented. It is obsrved that the inclusion of hyperons affects the nucleon and hyperon spin-orbit potential significantly. The neutron and hyperon (Λ, Σ^+, Σ^-) mean potentials are also displayed.

The bound class of n, p, Λ, Σ^+ and n, p, Λ, Σ^- are suggested within the RMF. The addition of lambda obviously increase the stability of the system but further addition of sigma hyperons leads to more stable system with increasing binding. The combinations of hyperons with nucleons for a particular system are suggested which will form the bound system with high strangeness and might be produced in heavy-ion reactions. The investi-

gation on hypernuclei with high strangeness is quite welcome because these type of system might be produced in high-energy heavy ion reactions near the future. These types of study of hypernuclei with multiple strangeness will provide us a basic input for neutron as well as hyperon star studies, which are the body of current interest.

ACKNOWLEDGMENTS

One of the author (MI) would like to acknowledge the hospitality provided by Institute of Physics, Bhubaneswar during the work.

[1] M. Denysz et. al. Nucl. Phys. **49**, 121 (1963).
[2] D. J. Prowse, Phys. Rev. Lett. **17**, 782 (1966).
[3] H. Takahashi et. al. Phys. Rev. Lett. **87**, 121502 (2001).
[4] O. Hashimoto and H. Tamura, Prog. Part. Nucl. Phys. **57**, 564 (2006).
[5] E. Hiyama, M. Kamimura, T. Motoba, T. Yamada and Y. Yamamoto, Phys. Rev. C **65**, 011301(R) (2001).
[6] E. Hiyama, M. Kamimura, T. Motoba, T. Yamada and Y. Yamamoto, Nucl. Phys. A **691**, 107c (2001).
[7] E. Hiyama, M. Kamimura, T. Motoba, T. Yamada and Y. Yamamoto, Mod. Phys. Lett. **18**, 95 (2003).
[8] E. Hiyama, M. Kamimura, T. Motoba, T. Yamada and Y. Yamamoto, Nucl. Phys. A **737**, 138 (2004).
[9] E. Hiyama, M. Kamimura, Y. Yamamoto, T. Motoba and T. A. Rijken, Prog, Theo. Phys. Suppl. **185**, 106 (2010).
[10] E. Hiyama, T. Motoba, T. A. Rijken and Y. Yamamoto, Prog, Theo. Phys. Suppl. **185**, 1 (2010).
[11] E. Hiyama, M. Kamimura, Y. Yamamoto, T. Motoba and T. A. Rijken, Prog, Theo. Phys. Suppl. **185**, 152 (2010).
[12] H. Nemura, S. Shinmura, Y. Akaishi, and Khin Swe Myint, Phys. Rev. Lett. **94**, 202502 (2005).
[13] H. Nemura, S. Shinmura, Y. Akaishi, and Khin Swe Myint, Nucl. Phys. A **754**, 110c (2005).
[14] A. Gal, Few. Body. Syst. **45**, 105 (2009).
[15] A. Gal and D. J. Millener, Phys. Lett. B **701**, 342 (2011).
[16] S. D. Randeniya and E. V. Hungerford, Phys. Rev. C **76**, 064308 (2007).
[17] A. A. Usmani, Phys. Rev. C **52**, 1773 (1995).
[18] A. A. Usmani, Phys. Rev. C **73**, 011302(R) (2006).
[19] A. A. Usmani and F. C. Khanna, J. Phys. G: Nucl. Part. Phys. **35**, 025105 (2008).
[20] Xian-Rong Zhou, A. Polls, H. -J. Schulze, and I. Vidaña, Phys. Rev. C **78**, 054306 (2008).
[21] I. Vidaña, A. Ramos and A. Polls, Phys. Rev. C **70**, 024306 (2004).
[22] C. Samanta, P. Roy Chowfhury and D. N. Basu, J. Phys. G: Nucl. and Part. Phys. **35**, 065101 (2008).
[23] C. Samanta and S. Adhikari, Nucl. Phys. A **738**, 491 (2004).
[24] C. Samanta and S. Adhikari, Phys. Rev C **65**, 037301 (2002).
[25] C. Samanta, P. Roy Chowfhury and D. N. Basu, J. Phys. G: Nucl. and Part. Phys. **32**, 363 (2006).
[26] B. F. Gibson, A. Goldberg and M. S. Weiss, Phys. Rev. C **6**, 741 (1972).
[27] B. F. Gibson and D. R. Lehman, Phys. Rev. C **37**, 679 (1988).
[28] R. H. Dalitz and B. W. Downs, Phys. Rev. **111**, 967 (1958).
[29] D. Vretenar, W. Pöschl, G. A. Lalazissis and P. Ring, Phys. Rev C **57**, R1060 (1998).
[30] H. F. Lü, J. Meng, S. Q. Zhong and S.-G. Zhou, Eur. Phys. J. A **17**, 19 (2003).
[31] A. Gal, Prog. Theor. Phys. Suppl., **186**, 270 (2010).
[32] A. Gal, Prog. Theor. Phys. Suppl., **156**, 1 (2004).
[33] M. Rufa, J. Schaffner, J. Maruhn, H. Stöcker and W. Greiner, Phys. Rev. C **42**, 2469 (1990).
[34] H. A. Bethe, G. E. Brown, and J. Cooperstein, Nucl. Phys. A **462**, 791 (1987).
[35] J. Ellis, J. I. Kapusta, and K. A. Olive, Nucl. Phys. B **348**, 345 (1991).
[36] N. K. Glendennning, F. Weber, and S. A. Moszkowski, Phys. Rev. C **45**, 844 (1992).
[37] M. Rufa, H. Stöcker, P. -G. Reinhard, J. Maruhn and W. Greiner, J. Phys. G: Nucl. Phys. **13**, L143 (1987).
[38] J. Mares and J. Zofka, Z. Phys. A **333**, 209 (1989).
[39] J. Schaffner, C. Greiner and H. Stoĉker, Phys. Rev. C **46**, 322 (1992).
[40] J. Schaffner, C. B. Dover, A. Gal, C. Greiner, D. J. Millener and H. Stöcker, Ann. Phys. (N.Y.) **235**, 35 (1994).
[41] J. Schaffner, C. B. Dover, A. Gal, C. Greiner and H. Stöcker, Phys. Rev. Lett. **71**, 1328 (1993).
[42] J. Schaffner-Bielich and A. Gal, Phys. Rev. C **62**, 034311 (2000).
[43] B. F. Gibson and E. V. Hungerford III, Phys. Rep. **257**, 349 (1995).
[44] E. Hiyama, Few. Body. Syst. **53**, 189 (2012).
[45] M. Rufa, J. Schaffner, J. Maruhn, H. Stöcker, W. Greiner and P. -G. Reinhard, Phys. Rev. C **42**, 2469 (1990).
[46] R. S. Hayano, T. Ishikawa, M. Iwasaki, H. Outa, E. Takada, H. Tamura, A. Sakaguchi, M. Aoki and T. Yamazaki, Phys. Lett. B **231**, 355 (1989).
[47] T. Nagae et al., Phys. Rev. Lett. **80**, 1605 (1998).
[48] V. G. J. Stoks and T. A. Rijken, Phys. Rev. C **59**, 3009 (1999).
[49] M. Prakash, I. Bombaci, M. Prakash, P. J. Ellis, J. M. Lattimer, and R. Knorren, Phys. Rep. **280**, 1 (1997).
[50] R. Knorren, M. Prakash, and P. J. Ellis, Phys. Rev. C **52**, 3470 (1995).
[51] J. Schaffner and I. Mishustin, Phys. Rev. C **53**, 1416 (1996).
[52] S. Balberg and A. Gal, Nucl. Phys. A **625**, 435 (1997).
[53] S. Balberg, I. Lichtenstadt, and G. B. Cook, Ap. J. Suppl. **121**, 515 (1999).
[54] H. -J. Schulze, M. Baldo, U. Lombardo, J. Cugnon, and A. Lejeune, Phys. Rev. **57**, 704 (1998); M. Baldo, G. F. Burgio, and H. -J. Schulze, Phys. Rev. C **58**, 3688 (1998).
[55] I. Vidaña, A. Polls, A. Ramos, L. Engvik and M. Hjorth-Jensen arxive:nucl-th/0004031v1 (2000).
[56] X. -R. Zhou, A. Polls, H. -J. Schulze and I. Vidaña, Phys. Rev. C **78**, 054306 (2008).
[57] M. T. Win, K. Hagino and T. Koike, Phys. Rev. C **83**, 014301 (2011).
[58] H. Shen, F. Yang and H. Toki, Prog. Theor. Phys. **115**, 325 (2006).
[59] S. Weissenborn, D. Chatterjee and J. Schaffner-Bielich,

Nucl. Phys. A **881**, 62 (2012).
[60] D. E. Lanskoy, Phys. Rev. C **58**, 3351 (1998).
[61] T. Harada, Nucl. Phys. A **754**, 86c (2005).
[62] W. Koepf and P. Ring, Z. Phys. A **339**, 81 (1991).
[63] B. D. Serot and J. D. Walecka, Adv. Nucl. Phys. **16**, 1 (1986).
[64] B. D. Serot, Rep. Prog. Phys. **55**, 1855 (1992).
[65] P. Ring, Prog. Part. Nucl. Phys. **37**, 193 (1996).
[66] R. K. Gupta, M. Balasubramaniam, S. Kumar, S. K. Patra, G. Münzenberg and W. Greiner, J. Phys. G: Nucl. Part. Phys. **32**, 565 (2006).
[67] B. K. Sharma, P. Arumugam, S. K. Patra, P. D. Stevenson, R. K. Gupta and W. Greiner, J. Phys. G: Nucl. Part. Phys. **32**, L1 (2006).
[68] S. K. Patra, R. K. Gupta, B. K. Sharma, P. D. Stevenson and W. Greiner, J. Phys. G: Nucl. Part. Phys. **34**, 2073 (2007).
[69] J. D. Walecka, Ann. Phys. (N.Y.) **83**, 491 (1974).
[70] J. Boguta and A. R. Bodmer, Nucl. Phys. A **292**, 413 (1977).
[71] G. A. Lalazissis, S. Karatzikos, R. Fossion, D. Pena Arteaga, A. V. Afanasjev and P. Ring, Phys. Lett. B **671** 36 (2009).
[72] J. Mares and B. K. Jennings, Phys. Rev. C **49**, 2472 (1994).
[73] C. M. Keil, F. Hofmann and H. Lenske, Phys. Rev. C **61**, 064309 (2000).
[74] F. Yang and H. Shen, arXiv:0802.1965v1[nucl-th] (2008).
[75] http://cds.cern.ch/record/796514?ln=en, Rep. No. EXT-2004-134 (2004).
[76] N. Guleria, S. K. Dhiman and R. Shyam, Nucl. Phys. A **886**, 171 (2012).
[77] S. K. Singh, M. Ikram and S. K. Patra, Int. J. Mod. Phys. E **22**, 1350001 (2013).
[78] J. A. Wheeler, unpublished.
[79] H. A. Wilson, Phys. Rev. **69**, 538 (1946).
[80] P. J. Siemens and H. A. Bethe, Phys. Rev. Lett. **18**, 704 (1967).
[81] C. Y. Wong, Phys. Lett. B **41**, 451 (1972).
[82] K. T. R. Davies, C. Y. Wong and S. J. Krieger, Phys. Lett. B **41**, 455 (1972).
[83] J. Decharge, J. -F. Berger, M. Girod and K. Dietrich, Nucl. Phys. A **716**, 55 (2003).
[84] M. Grasso, L. Gaudefroy, E. Khan, T. Niksic, J. Piekarewicz, O. Sorlin, N. Van Giai and D. Vretenar, Phys. Rev. C **79**, 034318 (2009).
[85] J. Decharge, J. -F. Berger, K. Dietrich and M. S. Weiss, Phys. Lett. B **451**, 275 (1999).
[86] W. Y. Zao et al., Chin. Phys. Lett. **28**, 102101 (2011).
[87] E. Khan, M. Grasso, J. Margueron, N. Van Giai, Nucl. Phys. A **800**, 37 (2008).
[88] H. F. Lü and J. Meng, Chin. Phys. Lett. **19**, 1775 (2002).
[89] W. Z. Jiang, Phys. Lett. B **642**, 28 (2006).
[90] J. Boguta and S. Bohrmann, Phys. Lett. B **102**, 93 (1981).
[91] J. V. Noble, Phys. Lett. B **89**, 325 (1980).
[92] D. Vretenar, W. Pöschl, G. A. Lalazissis and P. Ring, Phys. Rev. C **57**, R1060 (1998).
[93] R. Brockmann and W. Weise, Phys. Lett. B **69**, 167 (1977).
[94] S. Ajimura et. al., Phys. Rev. Lett. **86**, 4255 (2001).